SCIENTIFIC REPORTS

OPEN

SUBJECT AREAS:
ELECTRONIC PROPERTIES AND MATERIALS
TWO-DIMENSIONAL MATERIALS

Received
8 October 2014

Accepted
9 December 2014

Published
13 January 2015

Correspondence and requests for materials should be addressed to Y.L. (ylli@iccas.ac.cn)

Self-catalyzed Growth of Large-Area Nanofilms of Two-Dimensional Carbon

Xuemin Qian[1], Huibiao Liu[1], Changshui Huang[2], Songhua Chen[1], Liang Zhang[1], Yongjun Li[1], Jizheng Wang[1] & Yuliang Li[1]

[1]CAS Key Laboratory of Organic Solids, Beijing National Laboratory for Molecular Sciences (BNLMS), Institute of Chemistry, Chinese Academy of Sciences, Beijing, 100190, People's Republic of China, [2]Department of Materials Science & Engineering, University of Wisconsin-Madison, Madison, Wisconsin 53706, United States.

The graphdiyne (GD), a carbon allotrope with a 2D structure comprising benzene rings and carbon–carbon triple bonds, can be synthesized through cross-coupling on the surface of copper foil. The key problem is in understanding the dependence of layers number and properties, however, the controlled growth of the layers numbers of GD film have not been demonstrated, its controlled growth into large-area and high ordered films with different numbers of layers is still an important challenge. Here, we show that a new strategy for synthesizing GD films with 2D nanostructures on ZnO nanorod arrays through a combination of reduction and a self-catalyzed vapor–liquid–solid growth process, using GD powder as the vapor source and ZnO nanorod arrays as the substrate. HRTEM shows the distance between pairs of streaks being approximately 0.365 nm by different thicknesses of GD films. The approach enables us to construct large-area ordered semiconductive films with high-quality surfaces showing high conductivity (up to 2800 S cm^{-1}). FETs were fabricated based on the well ordered films; we prepared and measured over 100 devices. Devices incorporating these well-ordered and highly conductive GD films exhibited field-effect mobility as high as 100 cm^2 V^{-1} s^{-1}.

In recent years, all-carbon materials have been recognized as candidate materials for use in next-generation electronic and optoelectronic devices. Field-effect transistors prepared from carbon-based materials have attracted tremendous interest, predominantly because their unique electronic properties especially, high mobility suggest great potential for electronic applications[1–21]. Graphdiyne (GD), a new kind of carbon allotrope comprising benzene rings and carbon–carbon triple bonds (Figure 1a), can be synthesized through cross-coupling on the surface of copper foil[4]. In the GD structure, each benzene ring is connected to six adjacent benzene rings through two carbon–carbon triple bonds, resulting in a flat porous structure exhibiting high chemical stability and electrical conductivity. These triple bonds open up a potentially limitless array of geometries beyond the perfect hexagonal lattice of graphene[22–24]. Because GDs and graphynes display distinct electronic properties, with GDs possessing a band gap of 0.46 eV[22,23], they have attracted great interest for their use in the development of modern macro- and nano-electronics. Recent studies by Enyashin and Ivanovskii have indicated that GDs possess two-dimensional (2D) structures consisting of sp^2 and sp hybridized carbon atoms, with certain GDs possibly possessing Dirac cones[24]. Görling and colleagues studied the band structures of three graphynes—α-graphyne, β-graphynes and 6,6,12-graphyne—using state-of-the-art methods; their simulations revealed that each of these graphynes features Dirac cones, suggesting that graphynes and GDs might have unusual and potentially useful electronic properties[25]. Recently, Wang and colleagues reported the electronic structure of GD determined using X-ray absorption spectroscopy (XAS) and scanning transmission X-ray microscopy[26]. The hope is that GD can be used to produce new functional materials displaying distinct properties not exhibited by other carbon materials; it is, therefore, a good candidate material for developing electronic devices.

Herein, we report a new strategy for synthesizing GD films on ZnO nanorod arrays through vapor deposition, using GD powder as the vapor source and ZnO nanorod arrays as the substrate. The GD films we prepared exhibited high conductivities (up to 2800 S cm^{-1}). Devices incorporating these well-ordered and highly conductive GD films exhibited field-effect mobility as high as 100 cm^2 V^{-1} s^{-1}.

Results

The use of ZnO as a substrate was vital for the growth of uniform GD films. Reducing agents readily transform ZnO to elemental Zn, a metal possessing a relatively lower melting point, for use as a catalyst in the vapor–liquid–

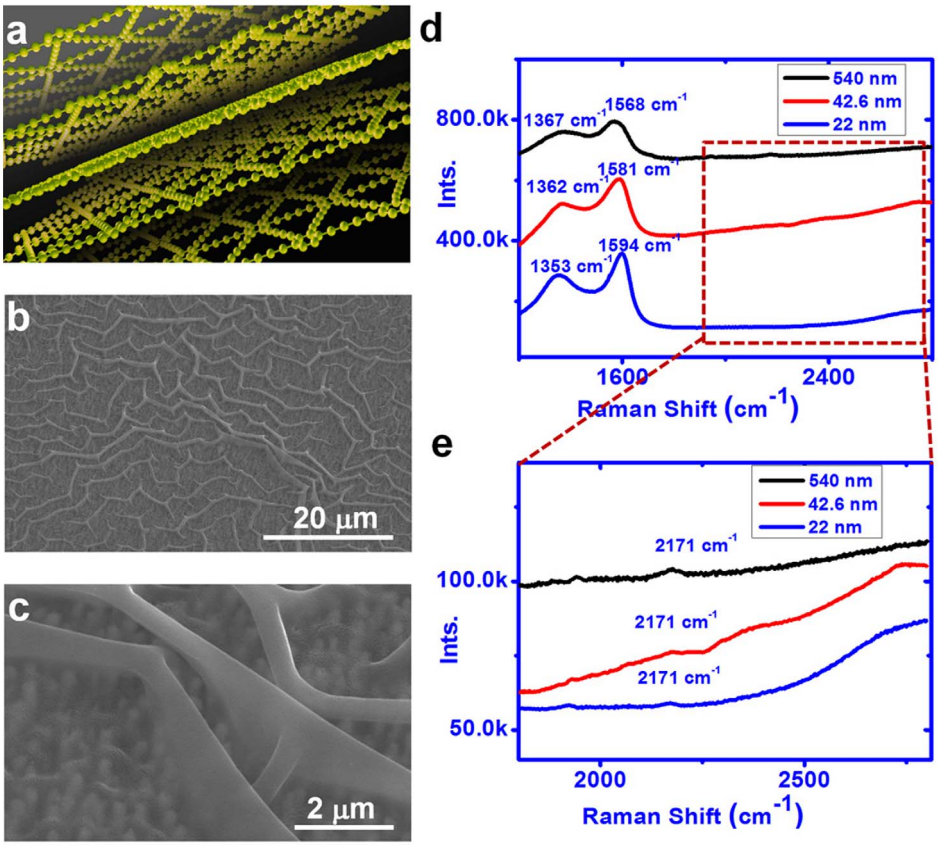

Figure 1 | A new strategy for synthesizing GD films with 2D nanostructures on ZnO nanorod arrays through a combination of reduction and a self-catalyzed vapor–liquid–solid growth process. (a) Model of the molecular structure of GD. (b), (c) Scanning electron microscopy (SEM) images of a continuous large-area GD film having a thickness of 540 nm (sample A): (b) lower magnification; (c) higher magnification. (d) Raman spectra of samples A, B, and C, displaying the four vibration peaks of the GD film respectively for the conjugated diyne groups. The intensity ratios (D/E_{2g}) for samples A, B, and C were 0.96, 0.87 and 0.83, respectively showing the GD films were highly ordered composed of multiple layers.

solid (VLS) growth process. We tested various substrates for their applicability in the growth of second layers of GD films, but the resulting films were non-uniform and disordered, except for those prepared using ZnO. The orientation of the ZnO nanorod arrays on the silicon slide was simple to control and could be used to induce the growth of orderly nanostructured films. Indeed, we found that the lower-molecular-weight GD could be evaporated from the diyne-polymer mixture to produce large-area ms with high-quality surfaces on the surfaces of the ZnO nanorod arrays.

To examine the potential practical applications of GD, we investigated the growth of GD films with different number of layers. When we placed 20 mg of GD powder into the quartz boat, we obtained a gray film on the surface of the ZnO nanorod arrays; the thickness of the GD film was approximately 540 nm (sample A) and its surface was very smooth (Figures 1b and 1c). This GD film was continuous over an area of greater than 4.8 mm^2. Figure 2a reveals that the average diameter of the ZnO nanorods aligned on the surface of the silicon slide and presenting a hexagonal smooth surface was approximately 500 nm. After decreasing the quantity of GD powder to 10 mg, we obtained a thinner GD film (sample B) having a thickness of 42.6 nm (Figure 2b). When we decreased the quantity of GD powder to 3 mg, the thickness of the as prepared GD film (sample C) decreased again (to 22 nm; Figure 2c). The as-prepared GD films (sample B) were transferred to one quartz glass substrate for measurement of UV-VIS-NIR spectrum (Figure S1). Figure S1 shows that the absorption peak at 2208 nm indicates a 0.56 eV optical band gap. The experimental value is in agreement with the calculated value (0.56 eV)[16].

Next, we used XPS and Raman spectroscopy to confirm the structures of the GD films of samples A. The XPS spectra of the sample A (Figure S2) featured similar C 1 s signals at 284.8 eV, which can be divided into three main sub-peaks at 284.5, 285.2, and 288.5 eV, attributable to the C 1 s orbital of C–C (sp^2), C ≡ C (sp), and C = O groups, respectively[4]. The area ratio of the signals for the sp- and sp^{2-} hybridized carbon atoms (ca. 2 : 1) confirmed that the benzene rings were linked together through diyne units in the as-prepared GD films. The Raman spectra of samples A–C (Figure 1d and 1e) display the characteristic peaks of the GD films. For sample A, four characteristic peaks of the GD film appeared at 1367, 1568, and 2171 cm^{-1}, respectively. The peak at 1568 cm^{-1} corresponds to the first-order scattering of the E_{2g} mode observed for in-phase stretching of the sp^2 carbon domains in aromatic rings; the peak at 1367 cm^{-1} represents the breathing vibration of sp^2 carbon domains in aromatic rings (the D mode)[4]. The intensity ratio (D/E_{2g}) of 0.96 indicated that the GD films were highly ordered and possessed low numbers of defects, and that the GD films were composed of multiple layers. The vibration peaks of conjugated diyne groups appeared at 2171 cm^{-1}[14]. Interestingly, the Raman vibrations of GD shifted to shorter wave-number upon decreasing the thickness of the GD film. For sample B, the D mode appeared at 1362 cm^{-1}, a hypsochromic shift relative to that of sample A (1367 cm^{-1}); the signals for the D modes of samples C and D—at 1353 and 1350 cm^{-1}, respectively—were shifted even further hypsochromically. The intensity ratios (D/E_{2g}) for samples B and D were 0.87 and 0.83, respectively.

We used atomic force microscopy (AFM) to probe the morphologies of the GD films on Si/SiO_2 substrates (Figure 2d–2f and Figure

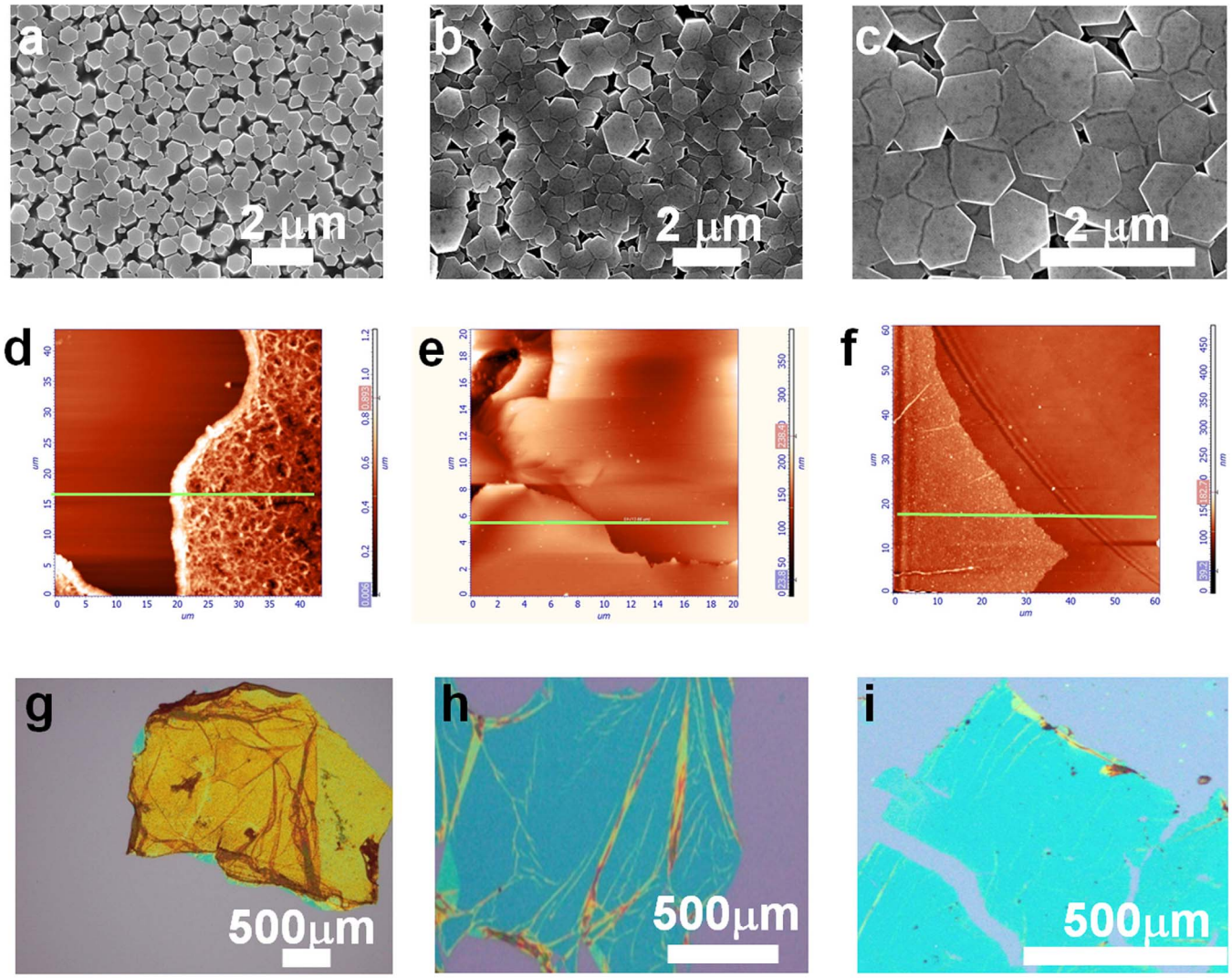

Figure 2 | The graphdiyne's controlled growth into large-area and high ordered films with different numbers of layers is achieved. SEM images of (a) ZnO NRs having a diameter of 500 nm and (b)–(d) GD films having thicknesses of (b) 42.6 nm (sample B) and (c) 22 nm (sample C). (d)–(f) AFM images of GD films of various thicknesses: (d) 540 nm (sample A), (e) 42.6 nm (sample B) and (f) 22 nm (sample C). (g)–(i) Optical microscopy images of GD films of various thicknesses, measured after transferring them onto SiO_2/Si substrates after dissolving the ZnO NRs: (g) 540 nm (sample A), (h) 42.6 nm (sample B), and (i) 22 nm (sample C).

S3). The cross-sectional height in Figure 2d reveals that the thickness of sample A was approximately 540 nm. The thicknesses of samples B and C were 42.6 and 22 nm, respectively (Figures 2e and 2f), corresponding to films derived from 58 and 30 layers of GD, respectively. Figures 2g–i present optical microscopy images of the three samples after their ZnO NRs had been dissolved and the films transferred onto SiO_2/Si substrates. The GD film from sample A was not transparent, due to its substantial thickness (540 nm) interfering with the permeation of light (Figure 2g). Upon proceeding from sample A to sample C, the GD films gradually became transparent, with the contrast with the substrate weakening (Figures 2g–i). The film grown from 3 mg of GD power exhibited high transparence and very low contrast with the substrate (Figure 2i). Thus, the growth of GD films could be controlled in terms of thickness by varying the quantity of GD powder used under the synthesis conditions.

We used transmission electron microscopy (TEM) and high-resolution transmission electron microscopy (HRTEM) to investigate the structures of the GD films. The images in Figures 3a–b reveal that sample A featured many clear streaks, with the distance between pairs of streaks being approximately 0.365 nm. Some curly streaks shown in Figure 3b further support that the streaks are not spacing lattice of GD film. To identify the crystallinity of the GD, we recorded selected-area electron diffraction (SAED) patterns from different sites of the GD films. We did not observe any diffraction spots in Figure S4a, suggesting that the GD films were amorphous. Fourier transform high-resolution transmission electron microscopy (FT-HRTEM) images (Figure S4b) further indicated that the streaks were not derived from the lattice of the crystal, but originated from the layer structure of the GD. The calculated interval between the two layers of GD was 0.365 nm, a distance greater than that of graphene[27–31]. The layer structures of the various GD samples could also be identified clearly in terms of their number of GD layers. Figures 3c–f reveal that samples B and C also exhibited layer structures having the same interval (0.365 nm).

We performed a number of experiments to confirm that the growth mechanism of the GD films could be described as a combination of a reduction and a self-catalyzed and saturated VLS model. The process, illustrated in Figure 4a, can be summarized as follows:

1) When the temperature at the center of the tube furnace was 700°C, GD powders of low molecular weight were evaporated and transported by the carrying gas to the low-temperature zone

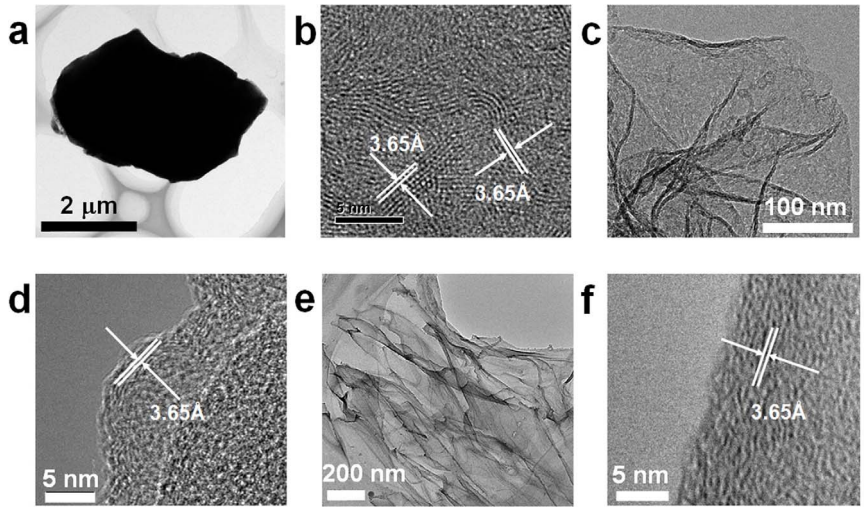

Figure 3 | **The transmission electron microscopy (TEM) and high-resolution transmission electron microscopy (HRTEM) to investigate the structures of the GD films, which show approximately distance of 0.365 nm between pairs of streaks by measurement of different thicknesses of 540 nm (sample A), 42.6 nm (sample B) and 22 nm (sample C) of GD films.** (a, c, e) TEM and (b, d, f) HRTEM images of samples: (a, b) sample A, (c, d) sample B, and (e, f) sample C.

(ca. 620°C) featuring a silicon substrate presenting ZnO NR arrays (Figure 4a–i, 4b–i and Scheme S1). The GD vapor reacted with the ZnO to form metallic Zn on top of the ZnO NRs. Simultaneously, the smooth surface (Figure 4c–i) at the top of the ZnO NRs became rougher with many kink sites produced as a result of the small amount of ZnO that had been reduced to metallic Zn (Figures 4c–ii and S5a). The rough surface and kink sites were conducive to 2D growth[32]. Some of the metallic Zn species were transported downstream by the carrying flow and some were deposited on top of the ZnO NRs, where the metallic Zn (melting point: 419°C) melted and condensed to form liquid droplets (Figure 4a–ii and 4b–i). Figure S6 reveals that the Zn transported downstream reformed into ZnO nanostructures on the surfaces of other ZnO NR arrays positioned far (ca. 12 cm) from the furnace centre, where the temperature was approximately 540°C (Scheme S1). The Zn droplets would act as catalysts in the VLS growth process. The arrows in Figures 4c-(iii–iv) and S7b–c highlight some of the ZnO nanoparticles in the GD films that originated from the reduced Zn droplets.

2) These Zn droplets acted as preferential, energetically favored sites for the adsorption of GD vapor[33]. A portion of the following GD vapor successively evaporated and dissolved in the Zn droplets, while another portion of the GD vapor continued to react with ZnO to form Zn. In this step, most of the GD vapor dissolved in the Zn droplets because the GD-mediated reduction of ZnO is not particularly fast at 700°C. Continuous dis-

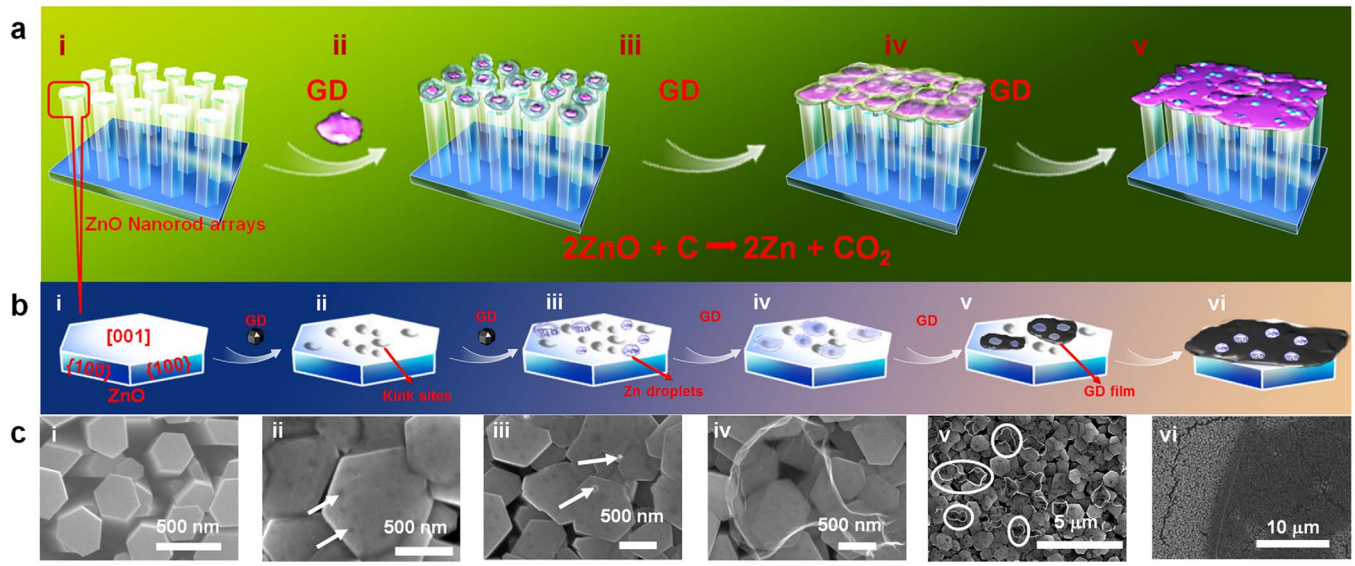

Figure 4 | (a) Schematic representation of the growth of a GD film, combining a reduction with a self-catalyzed and saturated VLS model. (b) Schematic representation of the growth of a GD film combining a reduction with a self-catalyzed and saturated VLS model on the top surface of a single ZnO NR. (c) SEM images corresponding schematic representation (b) of (i) ZnO NRs with smooth top surfaces and thin GD films; (ii) the rough surface and kink sites (marked with arrows) produced by ZnO reduced at the top of the ZnO NRs; (iii) ZnO nanoparticles, which originated from re-oxidized Zn droplets, scattered in the GD thin films; (iv) a typical droplet-like transparent GD thin film; (v) many small GD thin films, produced by a few Zn droplets, connected by two, three, or more pieces of smaller GD film; the morphologies of the small GD films are similar to those of the droplets; (vi) continuous large-area GD thin films.

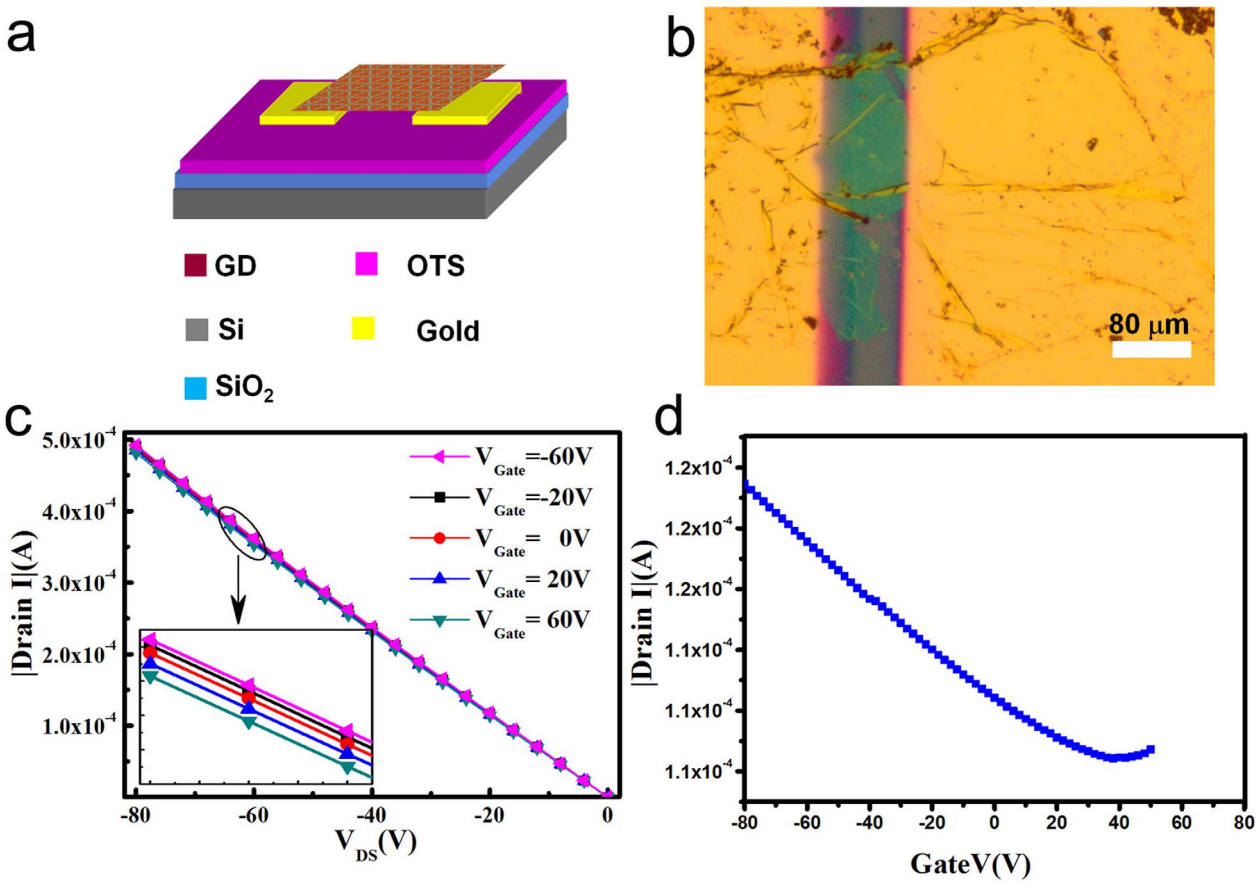

Figure 5 | (a) Schematic representation of the GD transistor. (b) Optical microscopy image of a GD FET device. (c) I_{ds}–V_{ds} characteristics of the device, the applied gate voltage (V_g) was in the range from −60 V (top) to 60 V (bottom). (d) Transfer characteristics, source–drain voltage held at a value of V_{ds} of −20 V.

solution of GD in the Zn droplets resulted in super saturation of GD in the Zn droplets, leading to segregation and the formation of GD nucleation sites (Figure 4b–iv and 4c–iii). For a crystalline material, growth in the VLS growth process generally occurs preferentially along the crystal face having the lowest surface energy[34], leading to formation of 1D nanostructures, the diameters of which are proportional to the ratio of the lateral and axial growth rates[35]. For an amorphous material, however, axial and lateral growths occur simultaneously, due to the absence of growth along any preferential crystal plane. The rate of lateral growth rate is determined by the super saturation ratio of the reagent species. In our case, the constant increase in the GD vapor pressure resulted in an increased super saturation ratio for GD in the droplets, a situation that is more conducive to lateral growth. The amount of droplets gradually increased as the reduction process proceeded. The GD molecules were dissolved at a constant rate in the Zn droplets, resulting in expansion of the diameters of the droplets and the interconnection of adjacent droplets, thereby facilitating lateral growth (Figure 4b–v and 4c–iv). In addition, a 2D material has a small edge energy, which also favors lateral growth[32,36]. Through a combination of all of these factors, the GD readily formed 2D film structures, rather than 1D nanostructures, on the top surfaces of the ZnO nanorods. Figures 4b–v and S5c–d reveal the gathering of regrown ZnO nanoparticles on the surfaces of GD films, confirming the phenomenon of the interconnection of adjacent Zn droplets (Figures S7a–h and S8a–c). Figure 4c–iv presents the image of a typical droplet-like GD thin film, which was transparent. From these findings, we conclude that the Zn droplets supersaturated with GD species expanded and syncretized to form continuous large-area GD films (Figures 4b–vi, 4c–vi, and S5e). The area of the thin GD film was low when the number of connecting Zn droplets was also low. Figures 4b–v and S7i–j reveal many small GD films connected by two, three, or more pieces of smaller GD films; the morphologies of these small GD films are similar to those of the droplets. For thick GD films, rupture could occur between GD films as a result of large tension (Figures S7f and S8g–h).

Amount of experiments about the growth results from different substrates, such as Si, silicon slide covered with a layer of Au, Ag, SiO_2, and ZnO nanopartilce film. We did not obtain the high quality GD films (Figure S9). In the process, the species of Au, Ag, Si and SiO_2 are not possible reduced by GD vapor to form liquid droplets for the GD films growth in VLS process. And then, the top of ZnO nanorod is a single crystal, which provides a large area smooth plane to load the Zn liquid droplets and connect them to form film; however, the ZnO nanoparticle films are without a large smooth plane to provide for loading the droplets.

To evaluate the electrical performance of GD films, we fabricated bottom-gate thin film transistors (TFT) on OTS/SiO_2/Si, with evaporation of Au electrodes directly on top of the GD films. Figure 5a is the schematic representation of the GD transistor. Figure 5b displays an optical image of the channel of a typical GD TFT having a channel length of 80 μm. We performed a systematic study of the electrical performance of the GD TFTs to examine their suitability as basic components in microelectronic integrated circuits and display electronics. We prepared and measured over 100 devices with an average mobility of 30 $cm^2 V^{-1} s^{-1}$. The conductivity of the GD film is rather high; Figure S10 reveals a GD film with a conductivity of 2800 S

cm^{-1}. Figure 5c and 5d show the output and transfer characteristics of the transistor, respectively. The output curves were not saturated, due to the conductivity of the GD film itself being very high; allowing us to calculate the hole linear mobility. The effective field effect mobility for the devices incorporating sample C was up to 100 cm^2 V^{-1} s^{-1}. In these measurements, the GD film materials exhibited double polarity, but it was very difficult to measure the n-type field effect behavior; nevertheless, we still obtained a few data exhibiting n-type field effect mobility, allowing us to calculate the average mobility. Although these field-effect mobility are much lower than those calculated theoretically for monolayer GD films (>1000 cm^2 V^{-1} s^{-1})[22,37], the major achievement in this paper is the first experimental demonstration of the field-effect mobility and semi-conductive features of GD materials. Further studies aimed at optimizing the properties of such GD films and their device architectures are currently underway. After optimizing the fabrication and measurement processes—for example, by using a shorter channel length or a better contact metal, or measuring under vacuum with the GD annealed under N_2—we expect that the device performances will be improved greatly.

Discussion

We have demonstrated a new strategy for synthesizing GD films on ZnO nanorod arrays through a combined reduction/self-catalyzed VLS growth process, using GD powder as the vapor source and ZnO nanorod arrays as the substrate. The GD films exhibited high conductivity (up to 2800 S cm^{-1}). Devices incorporating these well-ordered and highly conducting GD films exhibited field effect mobility as high as 100 cm^2 V^{-1} s^{-1}. Such systems might be of interest for fundamental nano-science and to applications in the field of nanotechnology.

Methods

Synthesis of GD films. The process used for the synthesis of GD films on ZnO nanorod arrays is presented in Scheme S1. The details regarding the synthesis of GD films on copper foil have been described elsewhere[4]. The newly formed diyne-polymers were mixtures of compounds of various molecular weights, resulting from different degrees of polymerization. The GDs of lower molecular weights were readily separated from the powdered mixture for further applications to the preparation of GD films on ZnO nanorod arrays, using a growth process combining reduction with a self-catalyzed and saturated VLS model.

As depicted in Scheme S1, a quartz boat containing an appropriate weight of the GD powder was placed into a quartz tube in a tube furnace. Argon (100 sccm) was introduced into the quartz tube for 60 min at room temperature to remove air; the flux of Ar was then turned to 60 sccm for use as the carrier gas. When the tube furnace temperature reached 700°C, the quartz boat was transferred to the center of the tube furnace. A silicon slide (1 × 2 cm^2) covered with a film of ZnO nanorod arrays was placed downstream, 8 cm away from the quartz boat. The temperature was maintained for 30 min and then the tube furnace was cooled to room temperature under a flow of high-purity N_2 (60 sccm). Gray films were formed on the surface of ZnO nanorod arrays film.

The experiments about the growth results from different substrates, such as Si, silicon slide covered with a layer of Au (thickness of 10 nm), Ag (thickness of 10 nm), SiO_2 (thickness of 200 nm), and ZnO nanopartilce film (thickness of 100 nm), were carried out by similar to the above procedure.

1. Kroto, H., Heath, J., O'Brien, S., Curl, R. & Smalley, R. C60: Buckminsterfullerene. *Nature* **318**, 162–163 (1985).
2. Iijima, S. Helical microtubules of graphitic carbon. *Nature* **354**, 56–58 (1991).
3. Novoselov, K. *et al.* Electric field effect in atomically thin carbon films. *Science* **306**, 666–669 (2004).
4. Li, G. *et al.* Architecture of graphdiyne nanoscale films. *Chem. Commun.* **46**, 3256–3258 (2010).
5. Hirsch, A. The era of carbon allotropes. *Nat. Mater.* **9**, 868–871 (2010).
6. Diederich, F. & Kivala, M. All-carbon scaffolds by rational design. *Adv. Mater.* **22**, 803–812 (2010).
7. Marsden, J. & Haley, M. Carbon networks based on dehydrobenzoannulenes. 5. Extension of two-dimensional conjugation in graphdiyne nanoarchitectures. *J. Org. Chem.* **70**, 10213–10226 (2005).
8. Dötz, F., Brand, J., Ito, S. Gherghel, L. & Müllen, K. Synthesis of large polycyclic aromatic hydrocarbons: Variation of size and periphery. *J. Am. Chem. Soc.* **122**, 7707–7717 (2000).
9. Feng, X. *et al.* Triangle-shaped polycyclic aromatic hydrocarbons. *Angew. Chem. Int. Ed.* **46**, 3033–3036 (2007).
10. Hoffmann, R. Extended Hückel theory. V. Cumulenes, polyenes, polyacetylenes and Cn. *Tetrahedron* **22**, 521–538 (1996).
11. Haley, M. Synthesis and properties of annulenic subunits of graphyne and graphdiyne nanoarchitectures. *Pure Appl. Chem.* **80**, 519–532 (2008).
12. Marsden, J., Palmer, G. & Haley, M. Synthetic strategies for Dehydrobenzo [n]–annulenes. *Eur. J. Org. Chem.* **13**, 2355–2369 (2003).
13. Bunz, U., Rubin, Y. & Tobe, Y. Polyethynylated cyclic π-systems: Scaffoldings for novel two- and three-dimensional carbon networks. *Chem. Soc. Rev.* **28**, 107–119 (1999).
14. Seol, J. *et al.* Two-dimensional phonon transport in supported graphene. *Science* **328**, 213–216 (2010).
15. Qian, X. *et al.* Construction of graphdiyne nanowires with high-conductivity and mobility. *Dalton Trans.* **41**, 730–733 (2012).
16. Wang, S. *et al.* A novel and highly efficient photocatalyst based on P25–graphdiyne nanocomposite. *Small* **8**, 265–271 (2012).
17. Li, Y. J., Xu, L., Liu, H. B. & Li, Y. L. Graphdiyne and Graphyne Based Materials—From Theoretical Predictions to Practical Construction. *Chem. Soc. Rev.* **43**, 2572–2586 (2014).
18. Li, G. *et al.* Construction of tubular molecule aggregations of graphdiyne for highly efficient field emission. *J. Phys. Chem. C* **115**, 2611–2615 (2011).
19. Liu, H., Xu, J., Li, Y. & Li, Y. Aggregate nanostructures of organic molecular materials. *Acc. Chem. Res.* **43**, 1496–1508 (2010).
20. Yang, N. *et al.* Photocatalytic properties of graphdiyne and graphene modified TiO_2: From theory to experiment. *ACS Nano* **7**, 1504–1512 (2013).
21. Sun, C. & Searles, D. Lithium storage on graphdiyne predicted by DFT calculations. *J. Phys. Chem. C* **116**, 26222–26226 (2012).
22. Long, M., Tang, L., Wang, D., Li, Y. & Shuai, Z. Electronic structure and carrier mobility in graphdiyne sheet and nanoribbons: Theoretical predictions. *ACS Nano* **5**, 2593–2600 (2011).
23. Luo, G. *et al.* Quasiparticle energies and excitonic effects of the two-dimensional carbon allotrope graphdiyne: Theory and experiment. *Phys. Rev. B* **84**, 075439 (2011).
24. Schirber, M. Focus: Graphyne may be better than graphene. *Physics* **5**, 24 (2012).
25. Malko, D., Neiss, C., Viñes, F. & Görling, A. Competition for graphene: Graphynes with direction-dependent Dirac cones. *Phys. Rev. Lett.* **108**, 086804 (2012).
26. Zhong, J. *et al.* Electronic structure of graphdiyne probed by X-ray absorption spectroscopy and scanning transmission X-ray microscopy. *J. Phys. Chem. C* **117**, 5931–5936 (2013).
27. Reina, A. *et al.* Large area, few-layer graphene films on arbitrary substrates by chemical vapor deposition. *Nano Lett.* **9**, 30–35 (2009).
28. Li, X., Wang, X., Zhang, L., Lee, S. & Dai, H. Chemically derived, ultrasmooth graphene nanoribbon semiconductors. *Science* **319**, 1229–1232 (2008).
29. Wang, X. *et al.* N-Doping of graphene through electrothermal reactions with ammonia. *Science* **324**,768–771 (2009).
30. Sun, Z. *et al.* Growth of graphene from solid carbon sources. *Nature* **468**, 549–552 (2010).
31. Tsen, A. *et al.* Tailoring electrical transport across grain boundaries in polycrystalline graphene. *Science* **336**, 1143–1146 (2012).
32. Yoshida, Y., Hirabayashi, I. & Takai, Y. Rapid growth of YBa2Cu3O7–y films by metalorganic chemical vapor deposition using vapor–liquid–solid mode. *J. Cryst. Growth* **229**, 348–352 (2001).
33. Barrelet, C., Wu, Y., Bell, D. & Lieber, C. Synthesis of CdS and ZnS nanowires using single-source molecular precursors. *J. Am. Chem. Soc.* **125**, 11498–11499 (2003).
34. Geng, C. *et al.* Well-aligned ZnO nanowire arrays fabricated on silicon substrates. *Adv. Funct. Mater.* **14**, 589–594 (2004).
35. Yan, Y., Zhou, L., Han, Z. & Zhang, Y. Growth analysis of hierarchical ZnO nanorod array with changed diameter from the aspect of supersaturation ratio. *J. Phys. Chem. C* **114**, 3932–3936 (2010).
36. Li, X. *et al.* Large-area synthesis of high-quality and uniform graphene films on copper foils. *Science* **324**, 1312–1314 (2009).
37. Kim, W. *et al.* Hysteresis caused by water molecules in carbon nanotube field-effect transistors. *Nano Lett.* **3**, 193–198 (2003).

Acknowledgments

This study was supported by the National Basic Research 973 Program of China (2011CB932302, 2012CB932901) and the National Nature Science Foundation of China (201031006 and 21290190). We thank Yuanchun Zhao (University of Wisconsin, Madison) for discussions regarding device fabrication.

Author contributions

Y.L.L. supervised the overall project. X.M.Q., H.B.L. and Y.L.L. conceived and designed the experiments. X.M.Q., H.B.L., C.S.H., S.H.C., Z.L., Y.J.L. and J.Z.W. performed the experiments. X.M.Q., H.B.L. and Y.L.L. discussed the results, analyzed the data, and wrote the manuscript.

Additional information

Supplementary information accompanies this paper at http://www.nature.com/scientificreports

Competing financial interests: The authors declare no competing financial interests.

How to cite this article: Qian, X. *et al.* Self-catalyzed Growth of Large-Area Nanofilms of Two-Dimensional Carbon. *Sci. Rep.* **5**, 7756; DOI:10.1038/srep07756 (2015).